The pyruvate dehydrogenase complex regulates mitophagic selectivity and matrix protein phosphorylation

Panagiota Kolitsida[1], Vladimir Nolic[1], Jianwen Zhou[2], Natalie M. Niemi[3], Jörn Dengjel[2] and Hagai Abeliovich[1]

1 Dept. of Biochemistry, Food Science and Nutrition, Hebrew University of Jerusalem, Rehovot, Israel

2 Department of Biology, University of Fribourg, Chemin du Musée 10, 1700 Fribourg, Switzerland

3 Department of Biochemistry and Molecular Biophysics, Washington University, St. Louis, MO

Address correspondence to: Dr. Hagai Abeliovich, Dept. of Biochemistry and Food Science, Hebrew University of Jerusalem, Rehovot, Israel 76100, Tel: 972-8-9489060; Fax: 972-8-9476189; E-mail: hagai.abeliovich@mail.huji.ac.il

Abstract

The mitophagic degradation of mitochondrial matrix proteins is selective, reflecting a pre-engulfment sorting step. This selectivity is regulated through phosphorylation of mitochondrial matrix proteins by the matrix kinases Pkp1 and Pkp2, which in turn appear to be regulated by the phosphatase Aup1/Ptc6. However, these same proteins also regulate the phosphorylation status and catalytic activity of the yeast pyruvate dehydrogenase complex, which is critical for mitochondrial metabolism. To better understand the relationship between these two functions, we evaluated the role of the pyruvate dehydrogenase complex in mitophagic selectivity. Interestingly, we identified a novel function of the complex in regulating mitophagy, which is independent of its enzymatic activity. Our data suggest an allosteric mechanism, wherein the pyruvate dehydrogenase complex directly regulates the activity of its cognate kinases and phosphatases to determine the phosphorylation state of mitochondrial matrix proteins and their mitophagic fate, in response to metabolic cues.

Keywords: mitophagy, protein phosphorylation, pyruvate dehydrogenase complex, mitophagic selectivity, Aup1, Pkp1, Pkp2

Introduction

Mitochondrial autophagy, or mitophagy, is a quality control mechanism that culls defective mitochondria in an effort to prevent cellular damage and dysfunction. Indeed, defects in mitophagic mechanisms have been shown to underlie human pathologies that can be traced to mitochondrial dysfunction. These include Parkinson's disease, Alzheimer's disease and type II diabetes (*1–3*). Known mitophagic mechanisms all involve a receptor protein which interacts with mitochondria on the one hand, and engages the autophagic machinery via LC3/Atg8 proteins and ancillary factors in response to specific cues, on the other hand (*4*). In mammalian cells, known mitophagy receptors include outer mitochondrial membrane (OMM) cardiolipin, NIX, BNIP3, NDP52, optineurin, prohibitin 2 , TAX1BP1, FUNDC1 and Bcl2-L-13 (*5–11*), all of which function under different induction conditions and in different cell types. In budding yeast cells, a single OMM protein, Atg32, functions as the only known mitophagy receptor (*12*, *13*). Current thinking envisions the selective activation of a mitophagy receptor on specific mitochondria, which leads to specific engulfment and degradation of those mitochondria. Thus, it is surprising that mitophagic processes, from yeast to man, exhibit protein level selectivity. We previously demonstrated, using SILAC-based proteomics and additional analyses, that different mitochondrial matrix proteins exhibit different mitophagic trafficking rates in yeast, and that this phenomenon correlates with physical segregation of the different proteins within the mitochondrial network (*14*). Similar observations were reported in human cells (*15*, *16*) and in drosophila (*17*, *18*). More recently, we found that protein phosphorylation in the mitochondrial matrix plays a role in determining intra-mitochondrial mitophagic selectivity. Briefly, we discovered that mitophagic trafficking of the phosphorylated reporter protein Mdh1-GFP depends on its phosphorylation status, and that phosphorylation of the relevant residues requires the function of the mitochondrial matrix kinases Pkp1 and Pkp2, acting under the regulation of the Aup1/Ptc6 phosphatase, which had previously been implicated in mitophagy (*19*, *20*).

Pkp1, Pkp2 and Aup1 have also been shown to regulate the phosphorylation of Pda1, the yeast E1α subunit of the mitochondrial pyruvate dehydrogenase complex (PDC) (*21–23*). One simple explanation for the data would be that the pyruvate dehydrogenase reaction, which generates acetyl-coA from pyruvate in the mitochondrial matrix, is required for mitophagy or for mitophagic selectivity. However, several problems arise with this hypothesis. For example,

in the regulation of pyruvate dehydrogenase activity, Pkp1 and Pkp2 function antagonistically relative to Aup1: they are required for phosphorylation of S313 on Pda1, which inactivates enzymatic activity, while Aup1 mediates dephosphorylation of this residue and activation of the enzyme (*22*). In contrast, in the regulation of Mdh1-GFP mitophagic trafficking, Pkp2 and Pkp1 function together with Aup1: both the kinases and the phosphatase are required for efficient mitophagy of several reporters, with the kinases functioning downstream of Aup1, as Pkp2 overexpression suppresses the *aup1Δ* phenotype (*19*).

To clarify and reconcile the relationship between the functions of Pkp1, Pkp2, and Aup1 in mitophagy versus their function in Pda1 regulation, we have now examined the potential role of the PDC in generating mitophagic selectivity. Surprisingly, the results of this investigation define a novel signaling cascade that is regulated by the PDC, but is uncoupled from its known enzymatic activity.

Results

Deletion of *PDA1* has a marked effect on mitophagic selectivity, which is uncoupled from pyruvate dehydrogenase activity

Since Aup1, Pkp1 and Pkp2 have been identified as pyruvate kinase phosphatases and kinases (*21–24*), we wanted to understand the relationship between their role in regulating mitophagic selectivity, and their role in regulating pyruvate dehydrogenase activity. Surprisingly, we found that deletion of the *PDA1* gene, which encodes the E1α subunit of the pyruvate dehydrogenase complex (PDC), has a major negative impact on the mitophagic trafficking of 5 different mitochondrial matrix proteins (Figure 1A, B). In contrast, the *pda1Δ* mutation had no effect on the mitophagic trafficking of an artificial mitophagy reporter, mtDHFR-GFP (Figure 1C, D), as we previously reported for the *pkp1Δ pkp2Δ* double mutant (*19*).

The most straightforward explanation for this result would be that the pyruvate dehydrogenase reaction itself, i.e. the formation of acetyl-CoA from pyruvate with concomitant reduction of NAD^+, is required for efficient mitophagy. However, deletion of the mitochondrial pyruvate carrier subunit *MPC1* had no effect on mitophagic trafficking (Figure 2A, B), even though this mutation prevents entry of pyruvate into mitochondria (*25*). We also tested whether the phosphorylation status of Pda1 at position Ser313 (the residue regulated by Pkp1/2 and Aup1;

(*21*, *22*)) directly determines mitophagic targeting. To this end, we determined whether deletion of *AUP1* can affect mitophagic trafficking in cells where the sole copy of *PDA1* encodes a serine to alanine mutation at position 313. As shown in Figure 2C and 2D, the Pda1^{S313A} mutant can weakly complement deletion of the WT protein for mitophagic trafficking of the Mdh1-GFP reporter. However, this residual mitophagic trafficking is completely lost in cells which also lack Aup1, indicating that Aup1 regulates mitophagic trafficking of Mdh1 independently of the phosphorylation state of serine 313 on Pda1. Finally, we tested whether catalytically inactive point mutations in the E1 and E2 subunits affect the mitophagic trafficking of the Mdh1-GFP reporter. For the E1α subunit Pda1, we chose the R322C mutation, which was previously shown to completely abrogate catalytic activity (*26*). As shown in Figure 2E and 2F, this point mutation caused a significant decrease in mitophagic trafficking of Mdh1-GFP, but still allowed a reproducible signal of free GFP under mitophagy inducing conditions, which was significantly higher than that observed in the deletion. Even more significantly, when we introduced the un-lipoylatable K75R mutation in the E2 subunit Lat1 (*27*, *28*), expression of this catalytically inactive mutant subunit led to a clear increase in mitophagic trafficking of Mdh1-GFP, completely opposite from the result expected if the *lat1Δ* phenotype was the result of a block in PDC catalytic activity (Fig. 2G, H). Collectively, these results indicate that the effects of the *pda1Δ* and *lat1Δ* mutations on mitophagic trafficking cannot simply be explained by the loss of PDC enzymatic activity, and are uncoupled from the phosphorylation state of Serine 313 on Pda1.

The PDC affects phosphorylation of Mdh1-GFP via regulation of Pkp1 and Pkp2

The extent of the decrease in mitophagic trafficking of mitochondrial matrix GFP chimeras, which we observe in *pda1Δ* cells (Figure 1A), is very similar to the phenotype which we had previously reported for the *pkp1Δ pkp2Δ* double mutant (*19*). Those previous studies showed that Mdh1-GFP is strongly hypo-phosphorylated in *pkp1Δ pkp2Δ* double mutants (*19*). An alternative hypothesis that we wanted to explore, was that the PDC reciprocally regulates its associated kinases and phosphatases, by virtue of their physical association (*22*, *23*, *29*), as such interactions could potentially allosterically regulate the enzymatic activities of Aup1, Pkp1 and Pkp2. If the effect of the *pda1Δ* mutation reflects a reciprocal regulation of Aup1, Pkp1 and Pkp2 by the PDC, we would expect that loss of Pda1 would similarly affect the phosphorylation of Mdh1-GFP. Indeed, we find that Mdh1-GFP phosphorylation is strongly attenuated in *pda1Δ* cells, and that this phenotype can be complemented by expressing Pda1 from a plasmid (Figure 3A, B). It was previously shown that Aup1 and Pkp1 stably interact with the PDC (*22*, *23*, *29*). To determine whether the PDC might function upstream of the kinases in regulating mitophagic trafficking of Mdh1-GFP, we tested if overexpression of Pkp1, Pkp2 or both kinases together, might rescue the mitophagy defect observed in *pda1Δ* cells. As shown in Figure 3C and 3D, co-overexpression of Pkp1 together with Pkp2, but not each kinase separately, causes a near complete rescue of the *pda1Δ* mitophagy phenotype. Co-overexpression of Pkp1 and Pkp2 also increases the phosphorylation of Mdh1-GFP in *pda1Δ* mutants, as would be expected if the PDC was modulating Pkp1/2 activity towards downstream targets (Figure 4A, 4B), and supporting our finding that it is not PDC catalytic activity which is affecting the mitophagic trafficking of Mdh1-GFP. We were also able to demonstrate a clear physiological function for Pkp1 and Pkp2 which is clearly distinct from the phosphorylation of the E1α subunit: While *pda1Δ* cells show a marked reduction in the percentage of colony forming cells following a prolonged incubation in respiratory medium, co-overexpression of Pkp1 and Pkp2 fully suppressed this phenotype (Figure 4C). This result demonstrates that the two kinases have a physiological function other than the regulation of PDC catalytic activity, and at the same time the epistatic relationship indicates- like our other results- that the PDC seems to act as an upstream regulatory element in these novel signaling pathways, independent of its catalytic activity.

If Pda1 regulates Mdh1-GFP phosphorylation via regulation of the activities of Pkp1 and Pkp2, then co-deletion of the opposing phosphatase should partially reverse this defect, as

any residual phosphorylation activity would now be amplified by the loss of the opposing phosphatase activity. Our previous work demonstrated that Aup1/Ptc6 cannot be opposing Pkp1/Pkp2 in regulating mitophagic trafficking, since 1) deletion of *AUP1* leads to a phenotype that is similar to the phenotypes of *PKP1Δ* and *PKP2Δ* on mutophagic trafficking, and 2) Aup1/Ptc6 functions upstream of Pkp2 in regulating Mdh1-GFP phosphorylation and mitophagic trafficking (*19*). We therefore tested the effects of deleting the mitochondrial phosphatases *PTC5* and *PTC7* (*22*, *30*) on Mdh1-GFP mitophagic trafficking, in the absence of Pda1. As shown in Figure 4D and 4E, deletion of *PTC5*, and to a much lesser extent deletion of *PTC7*, both led to some generation of free GFP in *pda1Δ* cells, while the phenotype of the combined *ptc5 pdc7* double deletion seems identical to the *ptc5Δ* phenotype. This result further supports the hypothesis that the PDC regulates the phosphorylation state of Mdh1-GFP, and identifies Ptc5 as the main phosphatase which antagonizes the function of Pkp1 and Pkp2 in regulating mitophagic trafficking of Mdh1-GFP.

To further test the possibility that conformational changes in the PDC may regulate Pkp1 and Pkp2 activity, we asked whether the catalytically inactive *lat1*^{K75R} mutation, which increases mitophagic efficiency of Mdh1-GFP (Figure 2G, H), also increased phosphorylation of this reporter. As shown in Figure 4F and 4G, deletion of *LAT1* decreased phosphorylation of Mdh1-GFP, while the K75R point mutation drastically increased phosphorylation of the protein, by 4-10 fold under these conditions, relative to the phosphorylation level in the WT control. Again, this result supports a conformation-dependent allosteric regulation of Pkp1/2 by the PDC, which is uncoupled from PDH catalytic activity.

We previously showed that deletion of Aup1, which functions upstream of Pkp2 in the cascade regulating mitophagic selectivity, leads to increased segregation of Mdh1-GFP relative to generic mtRFP, within the mitochondrial matrix (*19*). To test whether the deletion of *PDA1* similarly affects mitochondrial matrix heterogeneity, we compared the signal overlap between mtRFP and Mdh1-GFP in wild type and *pda1Δ* cells, over the first two days of incubation in SL medium (Figure 5). Wild-type cells show a slight, statistically insignificant decrease in signal overlap between day 1 and day 2 of the incubation. The *pda1Δ* mutant however, showed a statistically significant, ~40% reduction in signal overlap of Mdh1-GFP with mtRFP on day 2 relative to day 1 ($p<0.0001$), similar to what we previously observed for *aup1Δ* cells (*19*). Importantly, co-overexpression of Pkp1 and Pkp2 in the pda1Δ cells suppressed the decrease in signal overlap between days 1 and 2 of the incubation. In addition, we observed a mild

mitochondrial morphology phenotype in the *pda1Δ* strain, which appeared on day 2, in which both the red and the green signals appeared to be more clumped into a smaller number of larger foci relative to both WT and kinase-overexpressing strains.

Deletion of *PDA1* affects protein phosphorylation in the mitochondrial matrix.

Our experiments demonstrate a previously undescribed regulation of mitochondrial protein phosphorylation by the PDC. To determine whether loss of Pda1 can affect the phosphorylation state of additional mitochondrial matrix proteins, we carried out an unbiased phosphoproteomic screen to compare the phosphorylation state of mitochondrial proteins in the presence and absence of Pda1 under our working conditions. To this end, WT (heavy) versus *pda1Δ* (light) cells were differentially labelled with heavy and light isotope-substituted arginine and lysine. The cultures were collected on day 2 of an incubation in synthetic lactate medium (SL), the harvested cells were mixed in equal amounts, and mitochondria were enriched by differential centrifugation. As shown in Figure 6, we were able to identify 19 peptides derived from 8 mitochondrial matrix proteins, whose phosphorylation state was significantly and reproducibly affected by the deletion of *PDA1*. Interestingly, the list includes 3 mitochondrial tRNA ligases, the inner membrane ATP translocase, acyl carnitine transferase, a subunit of the mitochondrial H^+-ATPase, and a component of the electron transport chain. These results further indicate that PDC-mediated regulation of protein phosphorylation in the mitochondrial matrix is not limited to Mdh1.

Discussion

In this study, we have identified novel regulatory interactions between the pyruvate dehydrogenase complex and its attendant kinases. While previous studies, from the 1960's to the present, have focused on the fact that PDKs regulate pyruvate dehydrogenase activity (*21*, *22*, *31*, *32*), our data now demonstrate that the PDKs have additional substrates, and that their activity towards these non-PDC substrates can be reciprocally regulated by the PDC. This regulation may be mediated via allosteric interactions, as it was previously shown that Pkp1 and Pkp2 function as a heterodimer (*21*, *29*, *33*) and both Aup1 and Pkp1 stably interact with the PDC (*22*, *23*). Hundreds of mitochondrial matrix proteins have been documented to undergo phosphorylation (*34–36*). However, the nature of the signaling cascades involved and their regulation has remained obscure. Our discovery that Pkp1 and Pkp2 can function to phosphorylate a mitochondrial matrix protein other than Pda1 opens up the possibility that at least some of the documented phosphorylation events in the mitochondrial matrix are due to this novel regulatory axis. In support of this, we found by MS analysis that at least 8 additional mitochondrial matrix proteins show differential phosphorylation in response to deletion of Pda1 under our working conditions (Figure 6). We suggest that some of this regulation can be ascribed to an allosteric effect of the PDC on Aup1/Ptc6. As Aup1 has been shown to interact with the PDC (*22*), its phosphatase activity towards other substrates could be influenced by this stable physical interaction. Interestingly, the effects of *PDA1* deletion on matrix protein phosphorylation are diverse, with some sites hypophosphorylated and others hyperphosphorylated in *pda1Δ* cells, relative to WT (Fig. 5). In some cases, several peptides within the same protein (Yat1, Vas1) show opposite effects. This may reflect the confounding effects of parallel regulation of Aup1 on the one hand, and Pkp1/Pkp2 on the other hand. Alternatively, this may indicate that the regulation is not a simple on/off switch but rather a change in substrate specificity, bringing up the possibility that the association of Pkp1 and Aup1 with the PDC regulates substrate specificity, and not simply the activity of the kinases.

We propose, based on our data, that the PDC can function as a signaling hub which regulates protein phosphorylation in the mitochondrial matrix in response to metabolic cues (see model in Figure 7). We hypothesize that allosteric transitions within the PDC, induced by ligand or substrate binding, will affect the structure of the complex, leading to changes in the activity of its associated kinases and phosphatase(s). The entire system, including the redundancy of the pyruvate dehydrogenase kinases (there are 4 PDKs in mammals) and the

attendant PDC phosphatase, seems to be highly conserved. Strikingly, the region around the yeast Mdh1 phosphorylation site at Thr199 (IGGHSGITIIPPLISQ), which we previously showed to be crucial for mitophagic trafficking, is also highly conserved in human MDH2 (IGGHAGKTIIPLISQ) and the homologous Thr204 in the human protein was also reported to be phosphorylated (*37*). Therefore, it is likely that these reciprocal interactions are also conserved. Indeed, elegant biochemical studies from the Roche lab demonstrated that the activation of human PDK2 by NADH and acetyl coA was due to bound E2 becoming acetylated in the partial reverse reaction, demonstrating the existence of this exact type of allosteric coupling in human PDKs (*38*), although in that case, their conclusions limited the implication to the allosteric regulation of E1α phosphorylation. Our results now suggest a different interpretation for these previous findings. Similarly, it was recently reported that the overexpression of *PDK4* enhances mitophagy in mammalian cells (*39*) although again, the assumption was that this reflects regulation of pyruvate dehydrogenase activity. Another recent study found that branched-chain amino acids allosterically modulate PDC catalytic activity (*40*), supporting the notion that conformational changes in the PDC occur in response to metabolic cues. The results we have presented here suggest an additional dimension to the picture, by indicating that the PDC functions upstream of the PDKs to regulate mitochondrial function in response to such conformational changes.

The concept of large signaling complexes that integrate metabolic cues to regulate cellular activity has been the focus of intense study in recent years. TORC1 and TORC2 are example of such mega-complexes, which integrate nitrogen, amino acid and carbohydrate metabolism with hormone signaling, to generate readouts that regulate cellular responses to changes in the environment (*41–43*). We hypothesize that the PDC could serve a similar function within mitochondria, by regulating matrix protein phosphorylation in response to changes in metabolite levels. Further work will now be required to test specific aspects of this hypothesis.

Methods

Yeast strains, plasmids and growth conditions

Yeast strains used in this study are listed in Supplementary Table I. Deletion mutants and epitope-tagged strains were generated by the cassette integration method (*44*). Strain HAY75 (MATα *leu2-3,112 ura3-52 his3-Δ200 trp1-Δ901 lys2-801 suc2-Δ9*) was used as the WT genetic background in this study..

All knockout strains were verified by PCR. Oligonucleotides used in this study are detailed in Supplementary Table III, and plasmids are detailed in Supplementary Table II.

Yeast were grown in synthetic dextrose medium (0.67% yeast nitrogen base w/o amino acids (Difco), 2% glucose, auxotrophic requirements and vitamins as required) or in SL medium (0.67% yeast nitrogen base w/o amino acids (Difco), 2% lactate pH 6, 0.1% glucose, auxotrophic requirements and vitamins as required). All culture growth and manipulation were at 26 ^{0}C. Yeast transformation was according to Gietz and Woods (*45*).

For nitrogen starvation experiments, cells were grown to mid-log phase (OD_{600} of 0.4-0.6) in synthetic dextrose medium (SD), washed with distilled water, and resuspended in nitrogen starvation medium (0.17% yeast nitrogen base lacking amino acids and ammonium sulfate (Difco), 2% glucose) for the times indicated in individual experiments. Overexpression studies with *CUP1* promoter-based vectors were carried out by supplementing the medium with 5 μM $CuSO_4$, for both control (empty vector) and overexpressing cells.

Chemicals and antisera

Chemicals were purchased from Sigma-Aldrich (Rehovot, Israel) unless otherwise stated. Custom oligonucleotides were from Hylabs (Rehovot, Israel). Anti-GFP antiserum was from Santa-Cruz (Dallas, TX). Horseradish peroxidase-conjugated goat anti-rabbit antibodies were from MP Biomedicals (Santa Ana, CA). Anti-phosphoserine/threonine antibodies were from ECM Biosciences (catalog # PM3801).

Preparation of whole-cell extracts for western blot analysis

Cells (10 OD_{600} units) were treated with 10% cold trichloroacetic acid (TCA) and washed three times with cold acetone. The dry cell pellet was then resuspended in 100 μl cracking buffer (50 mM Tris pH 6.8, 6 M urea, 1 mM EDTA, 1% SDS) and vortexed in a Heidolf Multi Reax

microtube mixer at maximum speed with an equal volume of acid-washed glass beads (425-600μm diameter), for a total of 30 min. Lysates were clarified by centrifugation at 17,000 xg for 5 min and total protein was quantified in the supernatant using the BCA protein assay (Thermo Scientific, Rockford, IL). SDS loading buffer (final concentrations of 100 mM Tris pH 6.8, 20% glycerol, 2% SDS, 500 mM β-mercaptoethanol) was added to the lysate and the samples were warmed to 60 °C for 5 min prior to loading on gels. ImageJ software was used for band quantification.

Immunoblotting

SDS-10% polyacrylamide gels were transferred to nitrocellulose membrane by using either a wet or semidry blotting transfer system. Membranes were blocked for 1 h with TPBS (137 mM NaCl, 2.7 mM KCL, 10 mM Na_2HPO_4, 1.8 mM KH_2PO_4, 1 % Tween and 5 % milk powder (BD Difco Skim Milk), followed by incubation with rabbit anti-GFP (1:5000) for 1.5 h, then washed 4x 2 min with TPBS, incubated for 1.5 h with HRP conjugated secondary antibody (1:10000). The membranes were then washed 4x with TPBS, incubated with SuperSignal Chemiluminescence substrate (Thermo Scientific), and exposed to a Molecular Imager ChemiDoc™ XRS imaging system. Where necessary, 2% normal goat serum was added to blocking solutions to reduce background.

Calculation of statistical significance of differences in % free GFP signals from immunoblots

Data (% free GFP) were log-transformed before analysis in order to stabilize variances. A repeated measures ANOVA was performed to compare mutants and proteins simultaneously. Thereafter, mutants were compared for each protein and proteins were compared for each mutant by the Tukey HSD test ($p<0.05$). ANOVA analysis was carried out using JMP 12 software.

Native immunoprecipitation.

Cells (20 OD_{600} units) were washed 3x with 1 ml of cold 10 mM PIPES pH 7, 2 mM PMSF. The cell pellet was washed in three volumes of cold lysis buffer (20 mM HEPES pH 7.4, 50 mM NaCl, 1mM EDTA, 10% glycerol, 0.2 mM Na_3VO_4, 10 mM H_2NaPO_4, 10 mM β-glycerophosphate, 10 mM NaF, 10% phosphate cocktail inhibitors, 1 mM PMSF, proteases inhibitors (final concentrations: 5 μg/ ml antipain, 1 μg/ml aprotinin, 0.5 μg/ml leupeptin, 0.7

µg/ml pepstatin). The cells were then frozen in liquid nitrogen and stored at -80°C. Extracts were prepared from the frozen pellets using a SPEX Freezer/Mill according to the manufacturer's instruction. The frozen ground yeast powder was thawed at room temperature, and equal amount of lysis buffer plus Triton-X100 was added to a final concentration of 0.5% v/v detergent. Cell debris was removed by centrifugation at 17.000x g for 10 min at 4°C. 20 µl of GFP-Trap bead slurry (Chromotek) was pre-equilibrated in lysis buffer, per the manufacturer's instructions. The cleared lysate was added to the equilibrated beads and incubated for 1 h at 4 °C with constant mixing. The beads were washed five times with 1 ml ice cold wash buffer (20 mM HEPES pH 7.4, 50 mM NaCl, 0.5 mM EDTA, 10% glycerol, 0.5% Triton-X, 0.2 mM $NaOV_3$, 10 mM H_2NaPO_3, 10 mM β-glycerophosphate, 10 mM NaF, resuspended in 50 µl 2x SDS-loading buffer (200 mM Tris pH 6.8, 40% glycerol, 4% SDS, 1 M β-mercaptoethanol) and boiled for 10 min at 95°C. For phosphatase treatment, immunoprecipitated beads were incubated with 40 Units of lambda protein phosphate (New England Biolabs) in a 50 µl reaction. Samples were washed once with wash buffer and resuspended in 50 µl 2 x SDS-loading buffer.

SILAC labeling

To quantify relative phosphorylation on mitochondrial proteins in WT versus *pda1Δ* backgrounds, cell cultures of each strain were grown separately in SL medium supplemented respectively with 0.003% (w/v) $^{13}C_6\,^{15}N_2$ L-lysine (Lys8; Cat. Number 211604102, Silantes, Munich) and 0.001% (w/v) $^{13}C_6{}^{15}N_4$ L-arginine (Arg10; Cat. Number 201603902, Silantes, Munich) or with identical concentrations of unlabeled lysine and arginine, in addition to the standard auxotrophy supplementation. At the indicated time point, 50 OD_{600} units of cells from each labeling regime were combined, washed with cold lysis buffer, and cells were frozen in liquid nitrogen. To lyse the cells, the frozen suspensions were processed in a SPEX Freezer/ Mill according to the manufacturers' instructions. The frozen ground powder was thawed and clarified by centrifuging for 10 min at 500 xg. The clarified lysates were then further centrifuged for 10 min at 13,000 xg, the supernatant was discarded and the pellet was precipitated with 10% ice cold TCA and washed 3x with cold acetone.

MS analysis

Mass spectrometric measurements were performed on a Q Exactive HF-X mass spectrometer coupled to an EasyLC 1200 (Thermo Fisher Scientific, Bremen, Germany). Prior to analysis phosphopeptides were enriched on an Automated Liquid Handling Platform (AssayMap Bravo, Agilent) using Fe (III)-NTA cartridges (5 μL) essentially as described previously (PMID: 28107008). The MS raw data files were analysed by the MaxQuant software (*46*) version 1.4.1.2, using a Uniprot *Saccharomyces cerevisiae* database from March 2016 containing common contaminants such as keratins and enzymes used for in-gel digestion.

Statistical analysis

Phosphosite SILAC ratios were normalized to respective protein changes to discriminate regulated sites from regulated proteins. Measurements of three biological replicates (Pearson correlation of 0.64- 071) comparing WT to *pda1Δ* cells were averaged and log2 transformed. To determine sites that changed significantly between genotypes we calculated an outlier significance score on the merged log2-transformed phosphosite ratios according to (*46*) (significance A, $p<0.05$, BH corrected).

For statistical analysis of western blotting quantifications in Figures 3B, 4B, and 4G, % normalized phospho- AA signal intensity relative to GFP signal values were calculated from raw files. MANOVA was carried out for overall comparison of all the genotypes measured on three days (day 1, day 3 and day 5, N=3). Log-transformation of the data was applied before analysis to stabilize variances. Pairwise comparison of genotypes was carried out by contrast tests.

Site directed mutagenesis

Site directed mutagenesis protocol was carried out according to the Stratagene QuikChange system. *Pfu* DNA Polymerase (Fermentas) was used with a thermocycling protocol followed by removal of the parental strands with *DpnI* digestion. Thermocycling conditions were as follows: Initial denaturation at 95°C for 2 min, then (steps 2-4), 30 sec at 95 ^{o}C, 60 sec at 55 ^{o}C, and 12 min at 68 ^{o}C. Steps 2-4 repeated for 18 cycles. PCR products were treated with DpnI

(fermentas) for 1 hr at 37 °C, and precipitated using with 70% ethanol. DNA pellets were then dried and resuspended with 20 µl TE buffer pH 8. All mutagenesis products were transformed into *E. coli* DH5α and mutations were verified by sequencing. The oligonucleotide primers used to create site-directed MDH1-GFP variants and combined variants are listed in Supplementary Table III.

Fluorescence microscopy

Culture samples (3 µl) were placed on standard microscope slides and viewed using a Nikon Eclipse E600 fluorescence microscope equipped with the appropriate filters and a Photometrics Coolsnap HQ CCD. To achieve statistically significant numbers of cells per viewing field in the pictures, 1 ml cell culture was collected and centrifuged for 1 min at 3,500 xg prior to sampling. For quantitative analysis of co-localization, ImageJ software with the co-localization Plugin, JACoP (*47*) was used. Representative fields were analyzed in terms of channel intensity correlation coefficient.

For confocal microscopy**,** cells were placed on standard microscope slides and micrographs were obtained by confocal laser scanning microscopy using a Leica SP8, using a 63x water immersion lens. GFP excitation was carried out using the 488 nm line, and emission was collected between 500-540 nm. For RFP excitation we used the 552 nm line and fluorescence emission was collected between 590-640 nm.

For statistical analysis of channel overlap data, ANOVA analysis was carried out using JMP 16.0 software. Correlations were compared over mutations and days by two-factor ANOVA. As the mutation X day interaction effect was statistically significant ($p<0.0001$), the two days were compared for each mutation by contrast t-tests. Pre-planned comparisons to WT were also performed by contrast t-tests.

Acknowledgements

We wish to thank J.C. Martinou and Maya Schuldiner for discussions, Hillary Voet for help with statistical analysis, and Einat Zelinger for confocal microscopy. This work was funded by ISF grant 445/17 (to HA), GIF grant I-111-412.7-2014 (to HA and JD), the University and Canton of Fribourg and the Swiss National Science Foundation (J.D.).

Author contributions

P.K. planned experiments, carried out experiments, generated figures, and wrote the manuscript. V. N. carried out experiments. J.Z. carried out MS analyses. N.N. planned experiments and wrote the manuscript. J.D. carried out MS analyses, planned experiments, generated figures, and wrote the manuscript. H.A. Planned experiments, generated figures, and wrote the manuscript.

Bibliography

1. A. Metaxakis, C. Ploumi, N. Tavernarakis, *Cells* **7**, (2018).
2. C. Ploumi, I. Daskalaki, N. Tavernarakis, *FEBS J* **284**, 183 (2017).
3. S. B. Vafai, V. K. Mootha, *Nature* **491**, 374 (2012).
4. H. Abeliovich, J. Dengjel, *Biochem Soc Trans* **44**, 541 (2016).
5. I. Novak *et al.*, *EMBO Rep* **11**, 45 (2010).
6. G. Bellot *et al.*, *Mol Cell Biol* **29**, 2570 (2009).
7. R. L. Schweers *et al.*, *Proc Natl Acad Sci U S A* **104**, 19500 (2007).
8. M. Lazarou *et al.*, *Nature* **524**, 309 (2015).
9. L. Liu *et al.*, *Nat Cell Biol* **14**, 177 (2012).
10. Y. Wei, W. C. Chiang, R. Sumpter, P. Mishra, B. Levine, *Cell* **168**, 224 (2017).
11. T. Murakawa *et al.*, *Nat Commun* **6**, 7527 (2015).
12. T. Kanki, K. Wang, Y. Cao, M. Baba, D. J. Klionsky, *Dev Cell* **17**, 98 (2009).
13. K. Okamoto, N. Kondo-Okamoto, Y. Ohsumi, *Dev Cell* **17**, 87 (2009).
14. H. Abeliovich, M. Zarei, K. T. Rigbolt, R. J. Youle, J. Dengjel, *Nat Commun* **4**, 2789 (2013).
15. J. L. Burman *et al.*, *J Cell Biol* **216**, 3231 (2017).
16. R. H. Hämäläinen *et al.*, *Proc Natl Acad Sci U S A* **110**, E3622 (2013).
17. E. S. Vincow *et al.*, *Proc Natl Acad Sci U S A* **110**, 6400 (2013).
18. E. S. Vincow *et al.*, *Autophagy* 1 (2019).
19. P. Kolitsida *et al.*, *Proc Natl Acad Sci U S A* **116**, 20517 (2019).
20. R. Tal, G. Winter, N. Ecker, D. J. Klionsky, H. Abeliovich, *J Biol Chem* **282**, 5617 (2007).
21. U. Gey, C. Czupalla, B. Hoflack, G. Rödel, U. Krause-Buchholz, *J Biol Chem* **283**, 9759 (2008).
22. X. Guo, N. M. Niemi, J. J. Coon, D. J. Pagliarini, *J Biol Chem* **292**, 11751 (2017).
23. U. Krause-Buchholz, U. Gey, J. Wünschmann, S. Becker, G. Rödel, *FEBS Lett* **580**, 2553 (2006).
24. A. González, C. Casado, J. Ariño, A. Casamayor, *PLoS One* **8**, e64470 (2013).
25. S. Herzig *et al.*, *Science* **337**, 93 (2012).
26. S. Drakulic, J. Rai, S. V. Petersen, M. M. Golas, B. Sander, *Cell Mol Life Sci* **75**, 3009 (2018).
27. U. Gey, C. Czupalla, B. Hoflack, U. Krause, G. Rödel, *PLoS One* **9**, 103956 (2014).
28. J. E. Lawson, X. D. Niu, L. J. Reed, *Biochemistry* **30**, 11249 (1991).
29. A. Breitkreutz *et al.*, *Science* **328**, 1043 (2010).
30. X. Guo *et al.*, *Cell Rep* **18**, 307 (2017).
31. T. C. Linn, F. H. Pettit, L. J. Reed, *Proc Natl Acad Sci U S A* **62**, 234 (1969).
32. A. C. Cardoso *et al.*, *Nat Metab* **2**, 167 (2020).
33. C. Walter, A. Marada, C. Meisinger, *J Proteomics* **252**, 104430 (2022).
34. R. Kruse, K. Højlund, *Mitochondrion* **33**, 45 (2017).
35. J. Reinders *et al.*, *Mol Cell Proteomics* **6**, 1896 (2007).
36. M. Renvoisé, L. Bonhomme, M. Davanture, M. Zivy, C. Lemaire, *Methods Mol Biol* **1636**, 283 (2017).
37. A. N. Kettenbach *et al.*, *Sci Signal* **4**, rs5 (2011).
38. J. C. Baker, X. Yan, T. Peng, S. Kasten, T. E. Roche, *J Biol Chem* **275**, 15773 (2000).

39. S. Park *et al.*, *Cell Signal* **27**, 1824 (2015).
40. T. Li *et al.*, *Cell Metab* **25**, 374 (2017).
41. S. Eltschinger, R. Loewith, *Trends Cell Biol* **26**, 148 (2016).
42. A. Szwed, E. Kim, E. Jacinto, *Physiol Rev* **101**, 1371 (2021).
43. R. Nicastro, A. Sardu, N. Panchaud, C. De Virgilio, *Biomolecules* **7**, E48 (2017).
44. M. S. Longtine *et al.*, *Yeast* **14**, 953 (1998).
45. R. D. Gietz, R. A. Woods, *Methods Enzymol* **350**, 87 (2002).
46. J. Cox, M. Mann, *Nat Biotechnol* **26**, 1367 (2008).
47. S. Bolte, F. P. Cordelières, *J Microsc* **224**, 213 (2006).

Figure legends

Figure 1. **Loss of *PDA1* affects mitophagic trafficking and selectivity of mitochondrial matrix proteins**. WT and *pda1Δ* cells expressing the indicated GFP-tagged mitochondrial matrix proteins were grown in SL medium as indicated in "Methods". Samples were taken on days 1 and 5, and protein extracts were analyzed by anti-GFP immunoblotting. A. Loss of *PDA1* strongly attenuates mitophagic trafficking of Mdh1-GFP and this can be complemented by expressing Pda1 from a plasmid. B. Loss of *PDA1* strongly attenuates the mitophagic trafficking of endogenous GFP chimeras of five different mitochondrial matrix proteins. C. Loss of *PDA1* does not affect mitophagic trafficking of an artificial mitochondrial GFP fusion protein, mtDHFR-GFP. Deletion of *ATG32* is included as a negative control. D. Quantification of the data from (C). Data are shown from 3 independent biological replicates +/- standard deviation. ϕ denotes empty vector.

Figure 2. **The effects of *PDA1* deletion on mitophagy are not mediated through the pyruvate dehydrogenase reaction, and mitophagic trafficking can be modulated independent of S313 phosphorylation**. A. Loss of *MPC1* has no effect on mitophagic trafficking of Mdh1-GFP. WT, *mpc1Δ* and *pda1Δ* cells expressing Mdh1-GFP were grown in SL medium for the indicated amounts of time and protein extracts were generated. The extracts were analyzed by immunoblotting with α-GFP antibodies. B. Quantification of the data in A. C. Cells expressing the S313A Pda1 point mutant still exhibit an *AUP1*- dependent mitophagic trafficking phenotype despite the absence of phosphoserine 313. Cell handling was as in (A), but only the day 5 samples are shown. D. Quantification of the data in C. E. The catalytically inactive *pda1*^{R322C} mutant can support partial mitophagic trafficking of Mdh1-GFP. Only day 5 samples are shown for brevity. F. Quantification of the data in E. G. The unlipoylatable *lat1*^{K75R} mutant shows increased mitophagic trafficking of Mdh1-GFP, relative to WT. Only day 5 samples are shown, for brevity. G. Quantification of the data in F. All quantifications are presented as averages of 3 independent biological replicates with standard deviation depicted as error bars. ϕ denotes empty vector.

Figure 3. **The PDC regulates phosphorylation of Mdh1. A**. The *pda1Δ* mutation causes hypophosphorylation of Mdh1-GFP. WT and *pda1Δ* cells expressing Mdh1-GFP were grown in SL medium for the indicated amounts of time and protein extracts were generated and immunoprecipitated with α-GFP antibody. The immunoprecipitates were then probed with α-phosphoamino acid antibody (top panel) and α-GFP antibody (bottom panel). Right panel: day 5 samples were treated overnight with lambda phosphatase or mock treated as described in "Methods", and analyzed by immunoblotting. **B**. Quantification of the data in (**A**). The results of 3 independent biological repeats were quantified by normalizing the α-phosphoamino acid signal to the GFP signal, and averaging. **C**. Co-overexpression of Pkp1 and Pkp2 completely suppresses the mitophagy defect of *pda1Δ* cells. WT and *pda1Δ* cells expressing Mdh1-GFP as well as the indicated plasmids, were grown in SL medium for 5 days and protein extracts were generated. The extracts were analyzed by immunoblotting with α-GFP antibodies. **D**. Quantification of the data in (**C**). The results of 3 independent biological repeats were quantified by calculating the % free GFP relative to the total signal (N=3) and averaging. All experiments represent an average of at least 3 independent biological repeats and statistical analysis was carried out as described in Materials and Methods. NS= not significant; Asterisks denote significant ($p < 0.05$) differences.

Figure 4. **Mdh1-GFP phosphorylation and mitophagic trafficking are regulated by the PDC complex independent of the pyruvate dehydrogenase reaction**. A. Co-overexpression of Pkp1 and Pkp2 suppresses the Mdh1-GFP phosphorylation defect in *pda1Δ* cells. WT and *pda1Δ* cells expressing Mdh1-GFP as well as the indicated plasmids were grown in SL medium for the indicated amounts of time and protein extracts were generated and immunoprecipitated with α-GFP antibody. Phosphorylation of Mdh1-GFP was detected using α-phosphoamino acid antibody and total GFP signal in the immunoprecipitate was observed by immunoblotting with α-GFP antibody. ϕ denotes empty vector. B. Quantification of the data in (A). The results of 3 independent biological repeats were quantified by normalizing the α-phosphoamino acid signal to the GFP signal, and averaged. C. Pkp1 and Pkp2 have a physiological function independent of pda1 phosphorylation. Cells were grown to late log phase in SD medium, washed and equal cell numbers were resuspended in SL medium. Cell viability was measured by plating diluted aliquots on rich YPD medium after 5 days of incubation in SL medium.

Clearly, co-overexpression of Pkp1 and Pkp2 completely suppresses the defect in *pda1Δ* cells. D. Deletion of PTC5 partially suppresses the *pda1Δ* mitophagy defect. Mdh1-GFP- expressing WT, *pda1Δ,* and *pda1Δ* cells harboring co deletions of *PTC7*, *PTC5* or both, were incubated in SL medium for 5 days and protein extracts were generated. The extracts were analyzed by immunoblotting with α-GFP antibodies. E. Quantification of 3 independent biological repeats of the experiment shown in D. F. The catalytically inactive $Lat1^{K75R}$ mutant causes massive hyperphosphorylation of Mdh1-GFP. Mutant *lat1Δ* cells expressing the indicated plasmids as well as Mdh1-GFP, were grown in SL medium for the indicated amounts of time and protein extracts were generated and immunoprecipitated with α-GFP antibody. Phosphorylation of Mdh1-GFP was detected and quantified as in A. All experiments represent an average of at least 3 independent biological repeats and statistical analysis was carried out as described in Materials and Methods. NS= not significant; Asterisks denote significant ($p< 0.05$) differences.

Figure 5. **Deletion of *PDA1* affects the intra-mitochondrial distribution of Mdh1-GFP**.

A) Deletion of *PDA1* affects distribution of Mdh1-GFP within the mitochondrial matrix. Cells co-expressing Mdh1-GFP from the endogenous *MDH1* promoter and a generic mtRFP were imaged on days 1 and 2 of the incubation (to avoid interference from vacuolar signal from day 3 and up. Top panels) and the overlap between the red and green channels was quantified as described in 'Materials and Methods'. B. Graph showing quantification of the overlap between the two channels in WT and in *pda1Δ* cells, and indicating statistical significance (NS, not significant). Results are representative of three biological replicates. Scale bar =5 μm.

Figure 6. **Deletion of *PDA1* has general effects on protein phosphorylation in the mitochondrial matrix**. A. Overview of the methodology. WT cells and *pda1Δ* cells expressing mtRFP were grown for 2 days in SL medium containing heavy lysine+arginine (WT) or regular lysine+arginine (*pda1Δ*). Equivalent amounts of WT and *pda1Δ* cells were combined (see Materials and Methods) and cell extracts were generated by gentle cryomilling. The extract was further centrifuged at 13000 xg and the pellet was analyzed by microscopic examination (100x objective) to verify the enrichment of intact mitochondria relative to total extract (B). DIC images are included to verify the absence of intact cells. C. Quantitative

SILAC MS/MS comparison of mitochondrial phosphopeptides identified in WT and *pda1Δ* mutants. Significant hits are annotated by protein. Phosphorylated positions are denoted in superscript.

Figure 7. **Model for regulation of mitochondrial protein phosphorylation by the PDC.** We propose that the known stable physical interactions between Aup1 and Pda1 (ref. 22) and between Pkp1 and Pda1 (ref. 23) can function as an allosteric interface to regulate Aup1, Pkp1 and Pkp2 activity towards other proteins within the mitochondrial matrix. We previously showed that Pkp2 functions downstream of Aup1, and in this study we showed that co-overexpression of Pkp1 and Pkp2 completely overcomes the mitophagy defect in *pda1Δ* cells. It remains to be seen whether physiological PDC ligands can allosterically regulate phosphorylation in the matrix. Since we also showed that Aup1 functions upstream of Pkp2 in regulating mitophagy, and we now demonstrate that the mitophagy-related function of Aup1 is independent of Pda1 phosphorylation, we propose that Pda1- bound Aup1 functions downstream of Pda1 to transduce signals to the kinase(s) in the pathway, although theoretically Aup1 may also affect Pkp2 completely independent from Pda1.

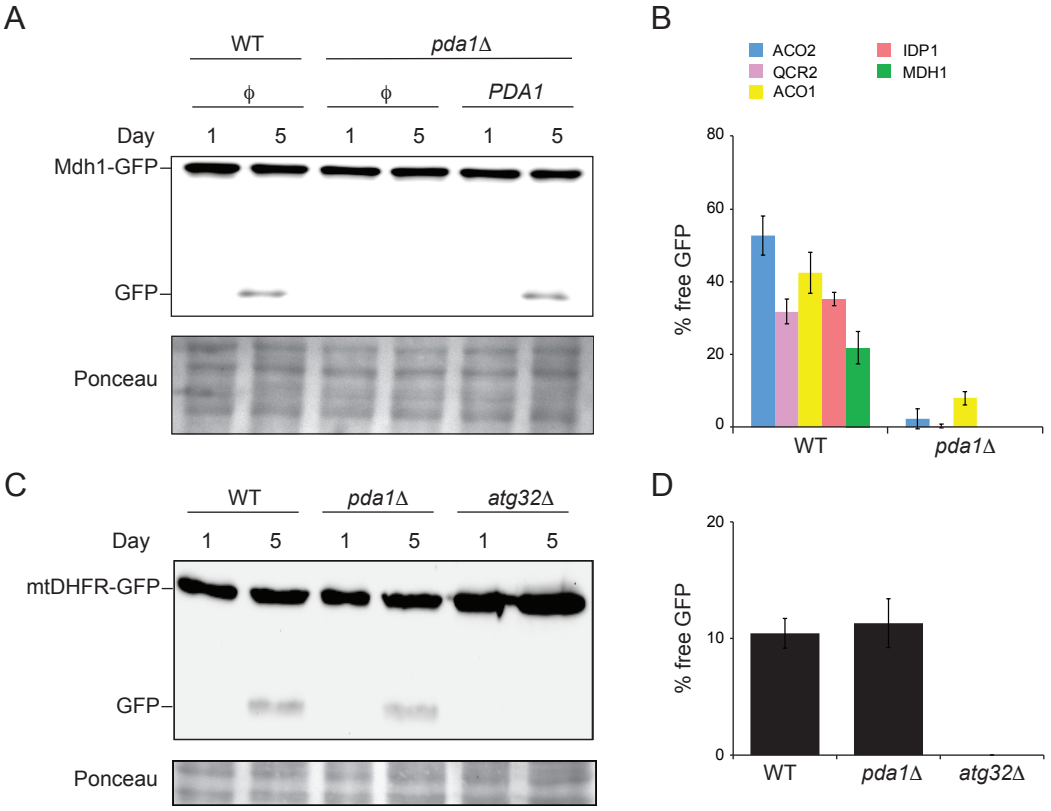
A
WT
pda1Δ
ϕ
ϕ
PDA1
Day
1
5
1
5
1
5
Mdh1-GFP
GFP
Ponceau
B
ACO2
QCR2
ACO1
IDP1
MDH1
% free GFP
80
60
40
20
0
WT
pda1Δ
C
WT
pda1Δ
atg32Δ
Day
1
5
1
5
1
5
mtDHFR-GFP
GFP
Ponceau
D
% free GFP
20
10
0
WT
pda1Δ
atg32Δ

Figure 1

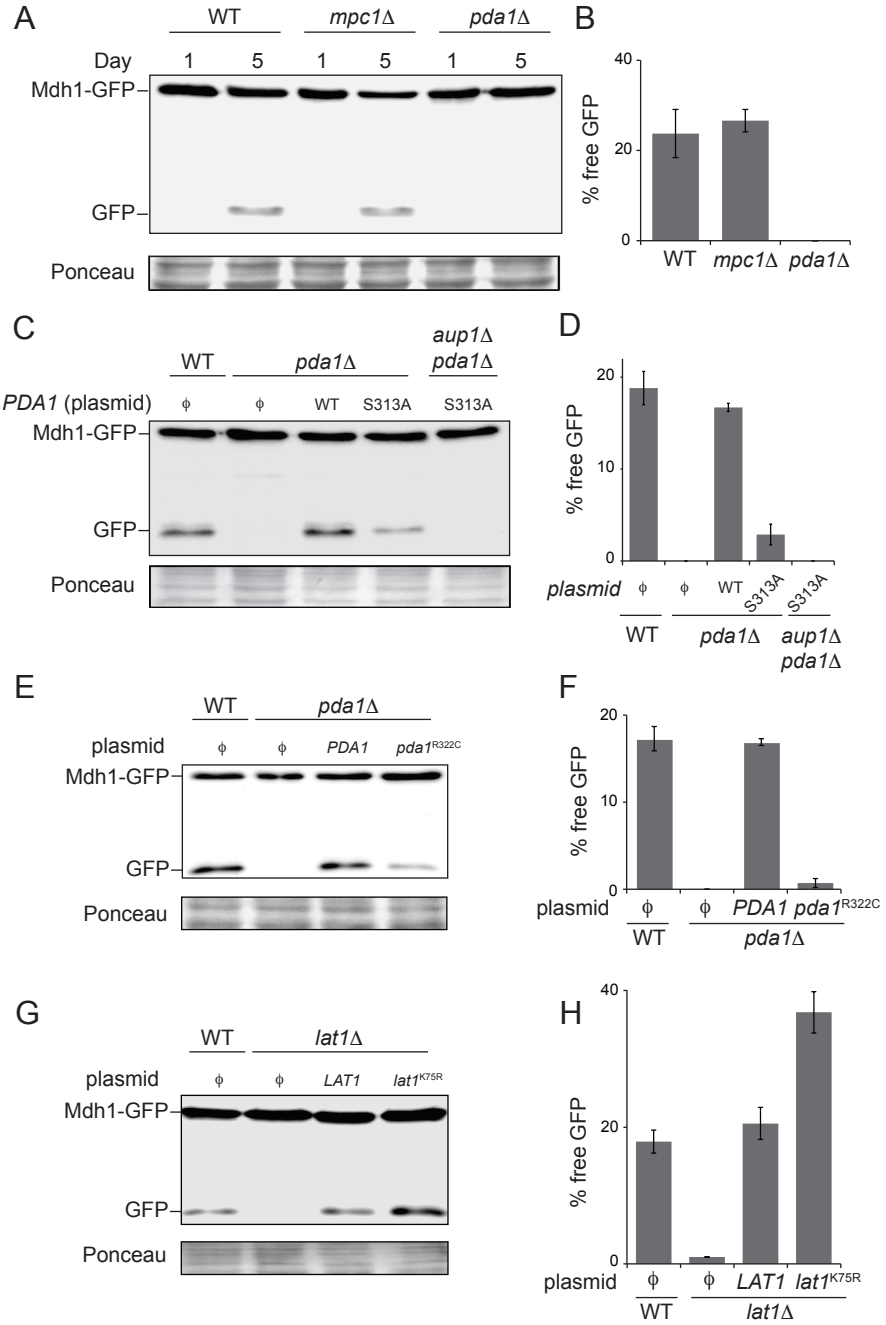
A
WT
mpc1Δ
pda1Δ
Day
1
5
1
5
1
5
Mdh1-GFP
GFP
Ponceau
B
% free GFP
40
20
0
WT
mpc1Δ
pda1Δ
C
WT
pda1Δ
aup1Δ pda1Δ
PDA1 (plasmid)
ϕ
ϕ
WT
S313A
S313A
Mdh1-GFP
GFP
Ponceau
D
% free GFP
20
10
0
plasmid
ϕ
ϕ
WT
S313A
S313A
WT
pda1Δ
aup1Δ pda1Δ
E
WT
pda1Δ
plasmid
ϕ
ϕ
PDA1
pda1R322C
Mdh1-GFP
GFP
Ponceau
F
% free GFP
20
10
0
plasmid
ϕ
ϕ
PDA1
pda1R322C
WT
pda1Δ
G
WT
lat1Δ
plasmid
ϕ
ϕ
LAT1
lat1K75R
Mdh1-GFP
GFP
Ponceau
H
% free GFP
40
20
0
plasmid
ϕ
ϕ
LAT1
lat1K75R
WT
lat1Δ

Figure 2

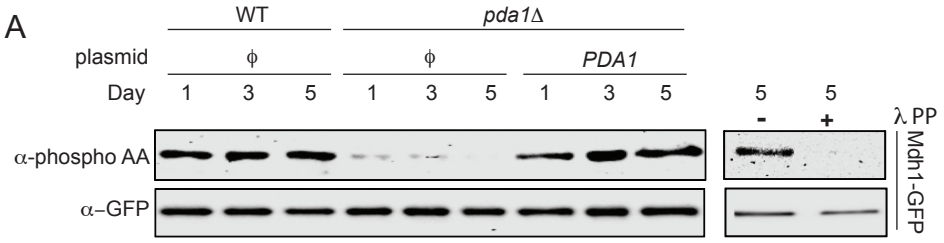
A
WT
pda1Δ
plasmid
ϕ
ϕ
PDA1
Day
1 3 5 1 3 5 1 3 5
5 5
- +
λ PP
α-phospho AA
α–GFP
Mdh1-GFP

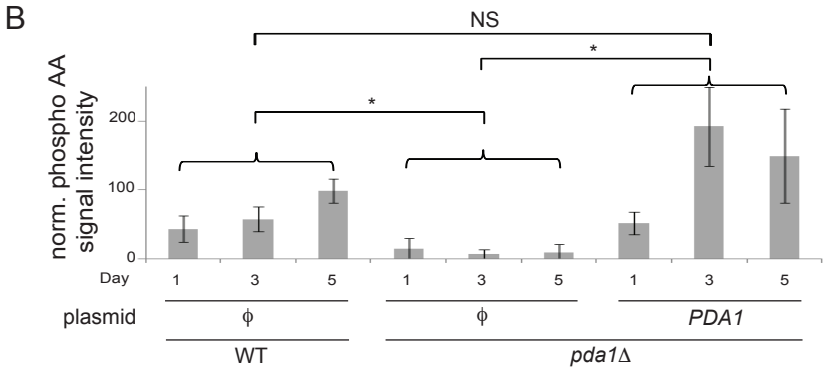
B
NS
*
*
norm. phospho AA signal intensity
200
100
0
Day
1 3 5 1 3 5 1 3 5
plasmid
ϕ
ϕ
PDA1
WT
pda1Δ

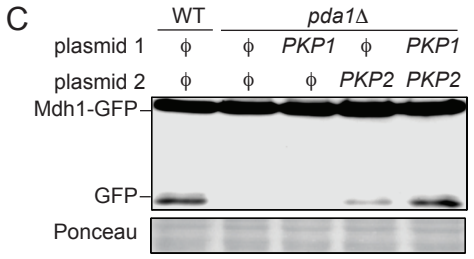
C
WT
pda1Δ
plasmid 1
ϕ ϕ PKP1 ϕ PKP1
plasmid 2
ϕ ϕ ϕ PKP2 PKP2
Mdh1-GFP
GFP
Ponceau

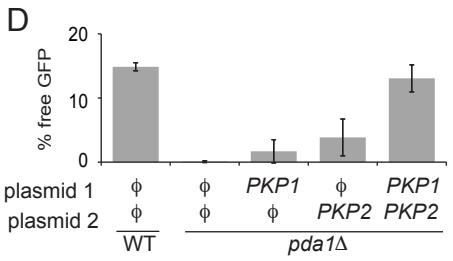
D
% free GFP
20
10
0
plasmid 1
ϕ ϕ PKP1 ϕ PKP1
plasmid 2
ϕ ϕ ϕ PKP2 PKP2
WT
pda1Δ

Figure 3

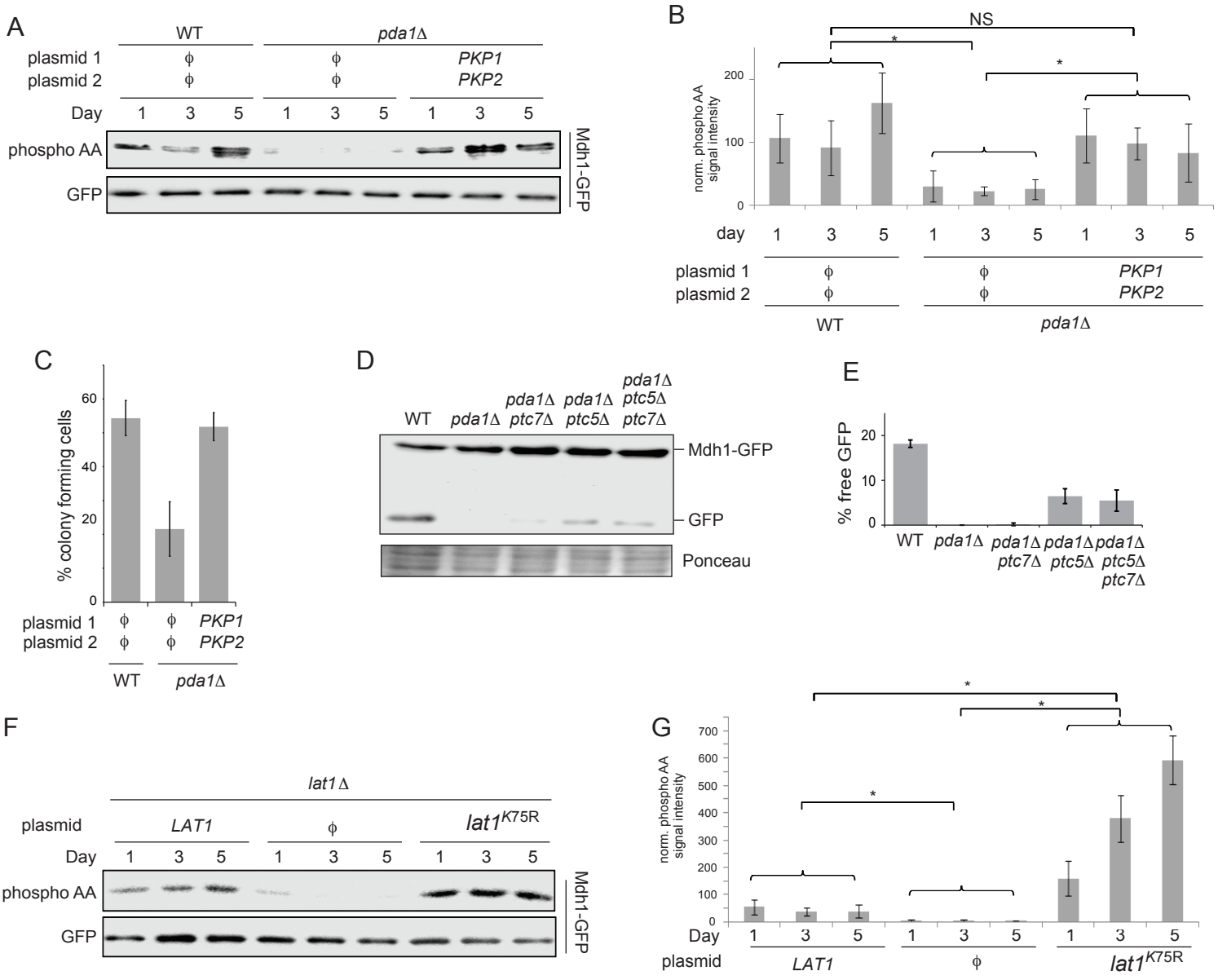
A
WT
pda1Δ
plasmid 1
plasmid 2
ϕ
PKP1
PKP2
Day
1 3 5 1 3 5 1 3 5
phospho AA
GFP
Mdh1-GFP
B
NS
*
norm. phospho AA signal intensity
200
100
0
day
1 3 5 1 3 5 1 3 5
plasmid 1
plasmid 2
ϕ
PKP1
PKP2
WT
pda1Δ
C
% colony forming cells
60
40
20
0
plasmid 1
plasmid 2
ϕ
PKP1
PKP2
WT
pda1Δ
D
WT
pda1Δ
pda1Δ ptc7Δ
pda1Δ ptc5Δ
pda1Δ ptc5Δ ptc7Δ
Mdh1-GFP
GFP
Ponceau
E
% free GFP
20
10
0
WT
pda1Δ
pda1Δ ptc7Δ
pda1Δ ptc5Δ
pda1Δ ptc5Δ ptc7Δ
F
lat1Δ
plasmid
LAT1
ϕ
lat1K75R
Day
1 3 5 1 3 5 1 3 5
phospho AA
GFP
Mdh1-GFP
G
*
norm. phospho AA signal intensity
700
600
500
400
300
200
100
0
Day
1 3 5 1 3 5 1 3 5
plasmid
LAT1
ϕ
lat1K75R

Figure 4

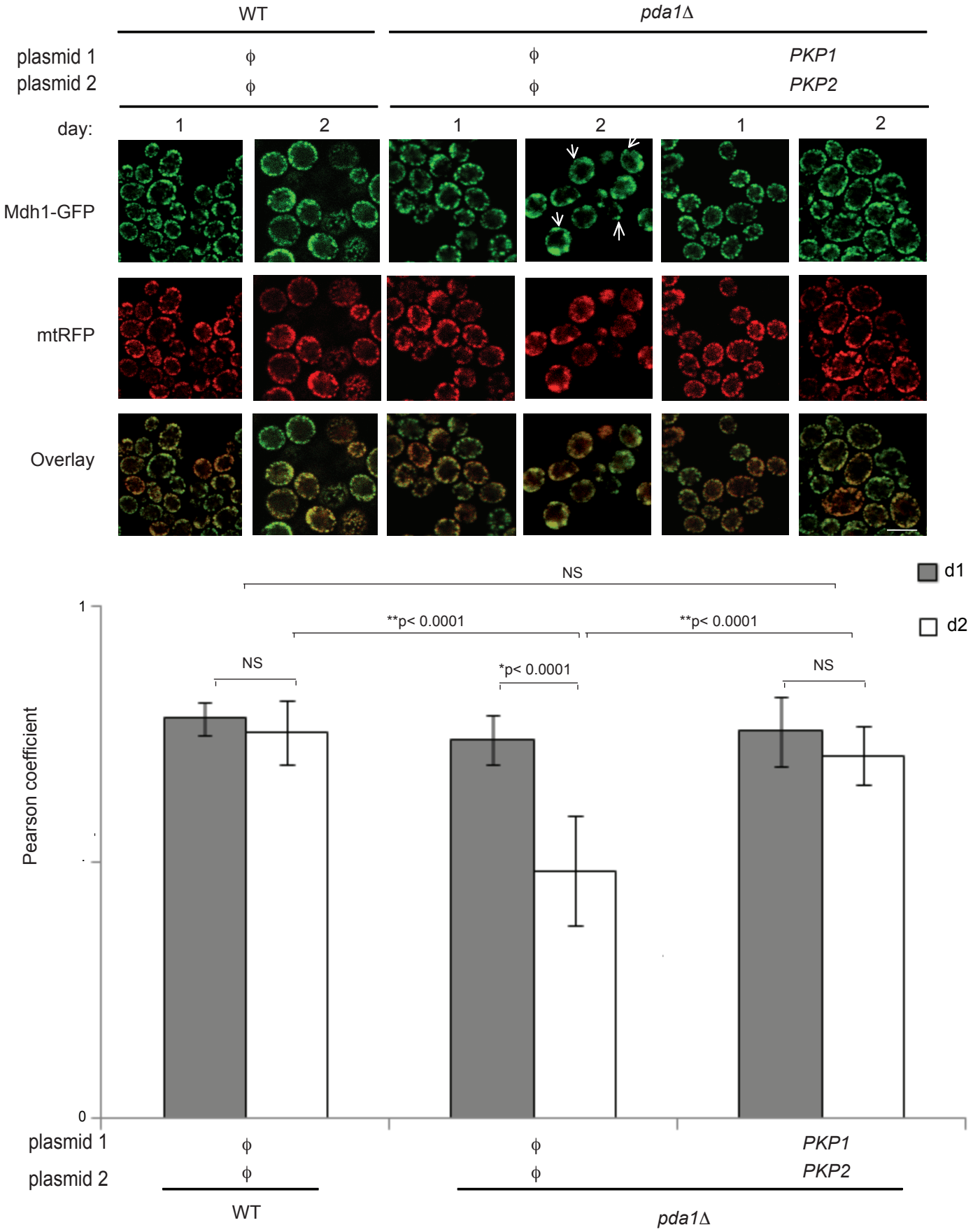
WT
pda1Δ
plasmid 1
plasmid 2
ϕ
ϕ
ϕ
ϕ
PKP1
PKP2
day:
1
2
1
2
1
2
Mdh1-GFP
mtRFP
Overlay
NS
**p< 0.0001
**p< 0.0001
NS
*p< 0.0001
NS
d1
d2
Pearson coefficient
1
0
plasmid 1
plasmid 2
ϕ
ϕ
ϕ
ϕ
PKP1
PKP2
WT
pda1Δ

Figure 5

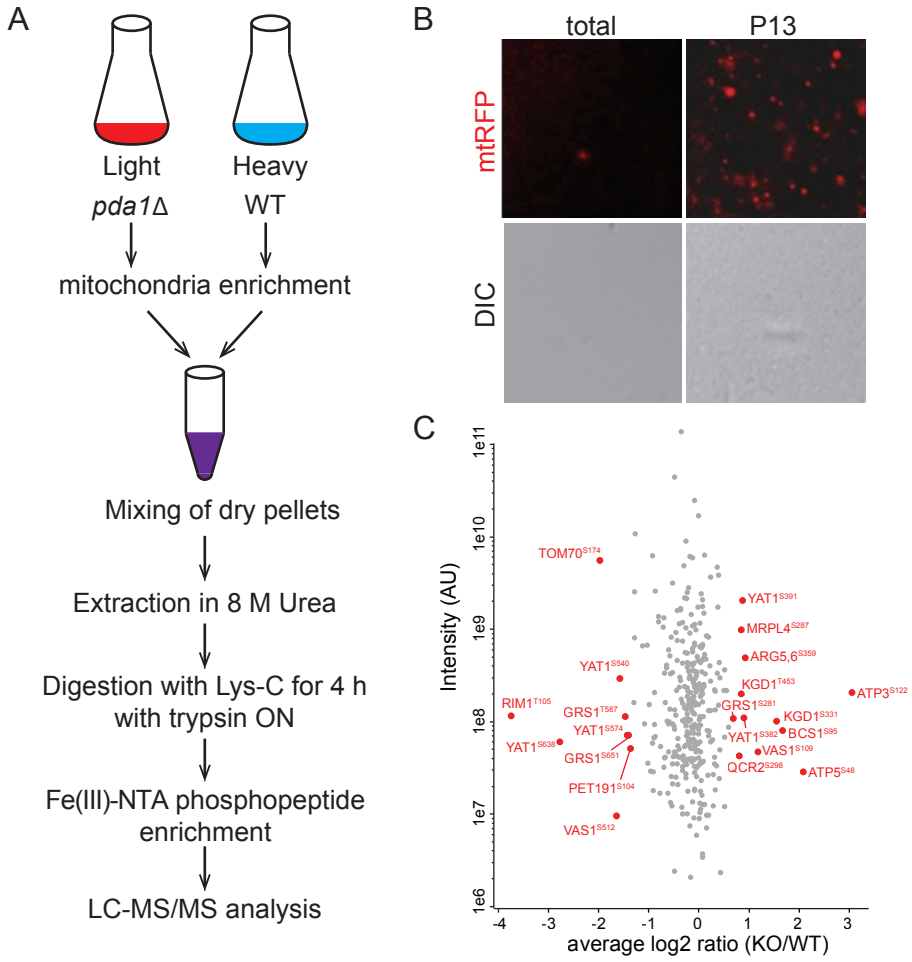
A
Light
pda1Δ
Heavy
WT
mitochondria enrichment
Mixing of dry pellets
Extraction in 8 M Urea
Digestion with Lys-C for 4 h
with trypsin ON
Fe(III)-NTA phosphopeptide
enrichment
LC-MS/MS analysis
B
total
P13
mtRFP
DIC
C
Intensity (AU)
average log2 ratio (KO/WT)
TOM70S174
YAT1S391
MRPL4S287
ARG5,6S359
YAT1S540
KGD1T453
ATP3S122
RIM1T105
GRS1T587
GRS1S281
KGD1S331
YAT1S574
YAT1S382
BCS1S95
YAT1S638
VAS1S109
GRS1S651
QCR2S298
ATP5S48
PET191S104
VAS1S512

Figure 6

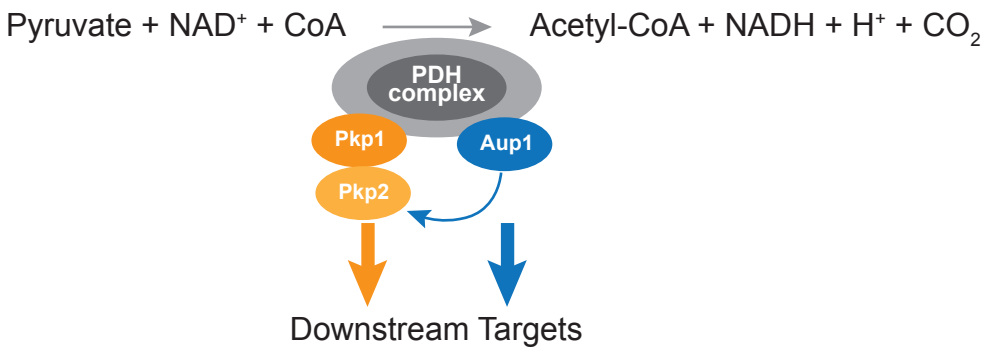
Pyruvate + NAD+ + CoA
Acetyl-CoA + NADH + H+ + CO2
PDH complex
Pkp1
Aup1
Pkp2
Downstream Targets

Figure 7

TABLE I. Yeast Strains used in this study

Strain	Genotype	Reference/source
***Saccharomyces cerevisiae* strains**		
HAY75 Wild type, progeny of SEY 6211 and SEY6210	*MATα leu2-3,112 ura3-52 his3-Δ200 trp1-Δ901 lys2-801 suc2-Δ9*	(Abeliovich et al. *Mol. Biol. Cell*, 2003)
PKY832	HAY75, *pda1Δ::HIS5 S.p.*	This study
HAY1239	HAY75, *atg32Δ::G418*^{R}	(Abeliovich et al., *Nat Commun,* 2013)
TVY1	HAY75*, pep4Δ::LEU2*	(Gerhardt et al., *J. Biol. Chem,* 1998)
PKY2046	HAY75, ACO2-GFP::*G418*^{R}	This study
PKY2047	HAY75, ACO1-GFP::*G418*^{R}	This study
PKY2045	HAY75, IDP1-GFP::*G418*^{R}	This study
PKY973	HAY75, QCR2-GFP::*G418*^{R}	This study
PKY974	HAY75, MDH1-GFP::*G418*^{R}	This study
PKY2041	PKY832, ACO2-GFP::*G418*^{R}	This study
PKY2041	PKY832, QCR2-GFP::*G418*^{R}	This study
PKY2023	PKY832, MDH1-GFP::*G418*^{R}	This study
PKY2044	PKY832, IDP1-GFP::*G418*^{R}	This study
PKY2063	PKY832, ACO1-GFP::*G418*^{R}	This study
PKY2089	HAY75, *mpc1Δ::HIS5 S.p.*	This study
PKY2104	PKY2089, MDH1-GFP::*G418*^{R}	This study
PKY1089	TVY1, MDH1 GFP::*G418*^{R}	This study
PKY1093	PKY1089:: *pda1Δ::HIS5 S.p*	This study
PKY2202	HAY75*, pep4Δ::*NAT^{R}	This study
PKY2206	PKY2202, *pda1Δ::HIS5 S.p*	This study
PKY2211	PKY2206, MDH1-GFP::*G418*^{R}	This study
PKY2216	PKY1089, pCU305::*LEU*, pCU306::*URA3*	This study
PKY2219	PKY2211, pCU305::*LEU*, pCU306::*URA3*	This study

PKY2220	PKY2211, PKP1 pCU305::*LEU*, PKP2 pCU306::*URA3*	This study
PKY2176	PKY974, pCU305::*LEU*, pCU306::*URA3*	This study
PKY2173	PKY2023, pCU305::*LEU*, pCU306::*URA3*	This study
PKY2072	PKY2023, pCU305::*LEU*, PKP2 pCU306::*URA3*	This study
PKY2071	PKY2023, PKP1 pCU305::*LEU*, pCU306::*URA3*	This study
PKY2070	PKY2023, PKP1 pCU305::*LEU*, PKP2 pCU306::*URA3*	This study
PKY520	TVY1, *arg4Δ:: G418*^{R}	This study
PKY2154	PKY520, mtDHFR-RFP pCU306::*URA3*	This study
PKY2196	PKY2154, *pda1Δ::HIS5 S.p*	This study
HAY809	HAY75, *aup1Δ::HIS5 S.p.*	Kolitsida et al, *PNAS,* 2019
PKY2088	HAY809, Mdh1-GFP::G418^{R}	This study
PKY2204	PKY2088, *pda1Δ::* NAT^{R}	This study
PKY2077	HAY75, *lat1Δ::HIS5 S.p.*	This study
PKY2083	PKY2077, MDH1-GFP::*G418*^{R}	This study
PKY15	*ptc5Δ::* NAT^{R}	Kolitsida et al, *PNAS,* 2019
PKY2239	PKY15, MDH1-GFP::*G418*^{R}	This study
PKY835	*ptc7Δ::HIS5 S.p.*	This study
PKY2234	PKY835, MDH1-GFP::*G418*^{R}	This study
PKY2252	PKY15, *pda1Δ::HIS5 S.p*	This study
PKY2284	PKY2252, *ptc7Δ:: DP*	This study
PKY2286	PKY2284, MDH1-GFP::*G418*^{R}	This study

TABLE II. Plasmids used in this study

Plasmid	Description	Backbone vector	RE sites in backbone vector/insert	Yeast Markers	Insert	Cloning Primers	Reference/ source
pCU416	-	-	*URA3*	-	-	-	(Labbe S et al.., 1999)
pRS415	-	-	*LEU2*	-	-	-	(Sikorsky R et al., 1989)
pCU306	-	-	*URA3*	-	-	-	(Labbe S et al.., 1999)
pCU305	-	-	*LEU2*	-	-	-	(Labbe S et al.., 1999)
pPKB138	pCU416-AUP1-HA	pCU416	ClaI, SpeI	*URA3*	AUP1	P1, P2	This study
pPKB78	pCU416-PDA1	pCU416	ClaI, SpeI	*URA3*	PDA1	P11,P12	This study
pPKB84	pCU416-*PDA1*^{S313A}	pCU416	ClaI, SpeI	*URA3*	PDA1	M1, M2	This study
pPKB89	pCU416-PKP1	pCU416	ClaI, SpeI	*URA3*	PKP1	-	Kolitsida et al, *PNAS,* 2019
pPKB132	pCU305-PKP1	pCU305	ClaI, SpeI	*LEU2*	PKP1	P5,P6	This study
pPKB90	pCU416-PKP2	pCU416	ClaI, SpeI	*URA3*	PKP2	-	Kolitsida et al, *PNAS,* 2019
pPKB133	pCU306-PKP2	pCU306	ClaI, SpeI	*URA3*	PKP2	P7, P8	This study
pKB115	pYX142 mt-DHFR-GFP	pYX142	BamHI, BglII	*LEU2*	Mt-DHFR-GFP	P9, P10	Kolitsida et al, *PNAS,* 2019
pPKB128	pCU306 mt-DHFR-RFP	pCU416	ECORI, BglII	*URA3*	Mt-DHFR-RFP	P3, P4	This study
PKB145	pRS414 LAT1	pRS414	PstI, SalI	*TRP*	LAT1	P13, P14	This study
PKB148	pRS414 LAT1^{K75R}	pRS414	PstI, SalI	*TRP*	LAT1	M5, M6	This study
PKB124	pCU416-*PDA1*^{R322Cys}	pCU416	ClaI, SpeI	*URA3*	PDA1	M3, M4	This study

TABLE III. Oligonucleotides used in this study

Primers	Purpose	Primers
P1	Amplification of AUP1-HA for the construction of pPKB138	Forward: 5' ATACTA ACTAGT TACAAC ATGCGGCTGGGGAATGCTTATG
P2		Reverse: 5' ATACTAATCGATTTACAATAGAATATAACCCA
P3	Amplification of mtDHFR-RFP for the construction of pPKB128	Forward: 5' ATACTAGAATTCTACAACATGGCCTCCACTCGTGTC
P4		Reverse: 5' ATACTA AGATCT GTCTTTCTTCTCGTAGAC
P5	Amplification of PKP1 for the construction of pPKB132	Forward: 5' ATACTAACTAGTTACAACATGTGGAAGATTATGCGTTC
P6		Reverse: 5' ATACTAATCGATTTACTTTTTGGAGAGTAGTG
P7	Amplification of PKP2 for the construction of pPKB90	Forward: 5' ATACTAGGATCCTACAACATGTCTAAGTATCAAATTAA
P8		Reverse: 5' ATACTAATCGATTCACACTTTATCTAATTGTAG
P9	Amplification of DHFR for the construction of pKB115	Forward: 5' ATACTAGGATCCTACAACATGATCAGTCTGATTGCGG
P10		Reverse: 5' ATACTAAGATCTCCGCCGCTCCAGAATCTC
P11	Amplification of PDA1 for the construction of pPKB118	Forward: 5' ATACTAACTAGTTACAACATGCTTGCTGCTTCATTC
P12		Reverse: 5' ATACTAATCGATTTAATCCCTAGAGGCAAAAC
P13	Amplification of LAT1 for the construction of pPKB145	Forward: 5' ATACTACTGCAGCTGTTTTCCAAGATATAC
P14		Reverse: 5' ATACTAGTCGACGTAAGTTCAAAAAGTTTG
D1	Amplification of *His5 S.p.* cassette for the deletion of *pda1Δ*	Forward: 5' GTTGGATACAGCAATAAGAAAGGAAACCACATTTGTGCCA CCCGGGCTGCAGGAATTC
D2		Reverse: 5' CGATCACAGCACTATTATTTTATTTTTCCTTACGATTTAA TCGACGGTATCGATAAGC
D3	Amplification natMX4 cassette for the deletion of *pep4Δ*	Forward: 5' ATTTAATCCAAATAAAATTCAAACAAAAACCAAAACTAAC CAGCTGAAGCTTCGTACG
D4		Reverse: 5' TATTGTTATCTACTTATAAAAGCTCTCTAGATGGCAGAAA CATAGGCCACTAGTGGATCTG
D5	Amplification of natMX4 cassette for the deletion of *pda1Δ*	Forward: 5' GTTGGATACAGCAATAAGAAAGGAAACCACATTTGTGCCACAG CTGAAGCTTCGTACG
D6		Reverse: 5' CGATCACAGCACTATTATTTTATTTTTCCTTACGATTTAA CATAGGCCACTAGTGGATCTG
D7	Amplification of *His5 S.p.* cassette for the deletion of *pdb1Δ*	Forward:5' TTTAGTAAGTTCTTTTACTTTTGCAATAATTTTGTTCAAC CCCGGGCTGCAGGAATTC
D8		Reverse:5' ATCTCCTTCTTTCTCTCCTTCCTATTGGATTGAAGTTTAT TCGACGGTATCGATAAGC

D9	Amplification of *His5 S.p.* cassette for the deletion of *lat1Δ*	Forward:5' GTAAACTGCATCCAGTAAAATTAATAGTTATTAGCGTACT CCCGGGCTGCAGGAATTC
D10		Reverse: 5' AGATACGCATTTACTGGCGAATTTTATTTTCATTCTAACC TCGACGGTATCGATAAGC
D11	Amplification of *His5 S.p.* cassette for the deletion of *pdx1Δ*	Forward:5' CTAGGTTATTGTTAAATCATCTCGAGGGAAAAATTCAAAA CCCGGGCTGCAGGAATTC
D12		Reverse:5' TGATAATGATAAACTCGAACTGAAAAAGCGTGTTTTTTAT TCGACGGTATCGATAAGC
D13	Amplification of *G418*^{R} cassette for the deletion of *arg4Δ*	Forward:5'GCTCAAAAGCAGGTAACTATATATAACAAGACTAAGGCGGTGGTCTTG CGCAACACG
D14		Reverse:5'CTAATTTAATTGGGATTTCAAATTATCCAATTGCTTCAATGAATTCGAGC TCGTTTAAAC
D15	Amplification of *His5 S.p.* cassette for the deletion of *mpc1Δ*	Forward:5' ATATATACGTATAGATTTTATTGCACTGTGATCAAAAAGA CCCGGGCTGCAGGAATTC
D16		Reverse:5' TCCATCTAGTCACCTACTTCAGGTTCTTAGACTGCTCGTT TCGACGGTATCGATAAGC
D17	Amplification of natMX4 cassette for the deletion of *ptc5Δ*	Forward:5' TTTCAACAGAAGAAGTGCTTTTACTTCTCT CAATCTCTCC3'
D18		Reverse:5' ATCCTCTGGTATATACCTACCTCAGCATAAGTTTATATC
D19	Amplification of *His5 S.p.* cassette for the deletion of *ptc7Δ*	Forward:5' ATAAAAGCGGTCCAGAAAACAAACGACAAAGCCACCAAAA
D20		Reverse:5'TTATTTACACTGCTTTCCAGGAGATTAAAGAGCGGAGTG
T1	Amplification of *His5 S.p.* cassette for the tagging of Aup1-HA	Forward: 5' CAAACTAATGAATGCACAATCTAACGAAACAAAATTAAAC TACCCATACGATGTTCCTG
T2		Reverse: 5' TCTTTCGATTAGCATCAAAAATCTCAGCATTTTTTCAGAA TCGACGGTATCGATAAGC
M1	Site Directed Mutagenesis of T313A on Pda1	Forward:5' GGTACGGTGGCCATGCTATGTCTGATCCC
M2		Reverse:5' GGGATCAGACATAGCATGGCCACCGTACC
M3	Site Directed Mutagenesis of R322Cys on Pda1	Forward:5' CCGGTACTACCTACTGAACTAGAGACGAG
M4		Reverse:5' CTCGTCTCTAGTTCAGTAGGTAGTACCGG
M5	Site Directed Mutagenesis of K75R on Lat1	Forward:5' CGAAATAGAAACAGACTCTGCTCAAATGGACTTTG
M6		Reverse:5' CAAAGTCCATTTGAGCAGAGTCTGTTTCTATTTCG